This is the peer reviewd version of the followng article:

Investigation of the behaviour of GaAs/AlGaAs SAM-APDs for synchrotron radiation / Nichetti, C., Steinhartova, T., Antonelli, M., Cautero, G., Menk, R.H., Pilotto, A., Driussi, F., Palestri, P., Selmi, L., Arfelli, F., Biasiol, G.. - (2019). (13th International Conference on Synchrotron Radiation Instrumentation, SRI 2018 Taipei International Convention Center, twn 2018) [10.1063/1.5084695].

Terms of use:

The terms and conditions for the reuse of this version of the manuscript are specified in the publishing policy. For all terms of use and more information see the publisher's website.

12/11/2026 09:20

(Article begins on next page)

Investigation of the Behaviour of GaAs/AlGaAs SAM-APDs for Synchrotron Radiation

Camilla Nichetti[1,2,a)], Tereza Steinhartova[2,3], Matias Antonelli[1], Giuseppe Cautero[1,4], Ralf Hendrik Menk[1,4,5], Alessandro Pilotto[6], Francesco Driussi[6], Pierpaolo Palestri[6], Luca Selmi[7], Fulvia Arfelli[2,4] and Giorgio Biasiol[3]

[1]*Elettra-Sincrotrone Trieste S.C.p.A, Area Science Park Basovizza, 34149 Trieste, Italy.*
[2]*Department of Physics, University of Trieste, 34128 Trieste, Italy.*
[3]*IOM CNR, Laboratorio TASC, Area Science Park Basovizza, 34149 Trieste, Italy.*
[4]*Istituto Nazionale di Fisica Nucleare, INFN Sezione di Trieste, Trieste, 34100, Italy.*
[5]*Department of Medical Imaging, University of Saskatchewan, Saskatoon, SK S7N 5A2, Canada.*
[6]*DPIA, University of Udine, Via delle Scienze 206, 33100 Udine, Italy.*
[7]*DIEF, University of Modena and Reggio Emilia, Via Trovarelli 2, 44100 Modena, Italy.*

[a)]Corresponding author: camilla.nichetti@elettra.eu

Abstract. This work reports on the fabrication and characterization of a novel high-speed, low-noise X-ray Avalanche Photodiode based on III-V compound semiconductors operating over an extended photon energy range. These materials were suggested as their higher atomic numbers allow for the absorption of higher photon energies; hence, shorter response times can be achieved by growing APDs with thinner active regions. In addition, the use of staircase hetero-junctions enhances electron multiplication and results in lower noise if compared with conventional p-i-n diodes. In this work, molecular beam epitaxy was used to produce GaAs/AlGaAs APDs with separated absorption and multiplication regions. The multiplication region, separated from the absorption region by a δ p-doped layer of carbon, contains a staircase structure composed of nanometric layers of AlGaAs and GaAs, which alternate periodically. The periodic modulation of the band gap enables a well-defined charge multiplication and results in low multiplication noise. Several devices were characterized in terms of dark current, photocurrents generated utilizing visible and hard X-ray sources as well as noise generated under laser light.

INTRODUCTION

Avalanche Photodiodes (APDs) are electronic devices which are designed to capture extremely low photon fluxes and convert them into measurable electric currents. When they are reverse biased near the breakdown voltage, the impact ionization mechanism amplifies the signal obtaining high gains without excessive additional noise, giving an advantage with respect to external electronical amplification.

Commercially available APDs for the wavelength range from infrared to ultraviolet are mainly made of Si as well as of compound semiconductors. On the contrary, APDs for detection in the X-ray regime, especially for applications in synchrotron radiation experiments, have been traditionally based on Si as it is the most mature technology and it has provided adequate performances. However, the characteristic of last-generation light sources has posed more stringent requirements in terms of detectable energies, response times and radiation hardness and this has led to the research of new materials. Compound-semiconductor APDs (e.g. based on GaAs/AlGaAs hetero-junctions) possess some advantages compared to Si and some promising developments reported in literature have led in this direction [1, 2]. In particular the high atomic number (Z_{Ga}=31 and Z_{As}=33) renders the GaAs absorption coefficient much higher than that of Si (Z_{Si}=14) [3]. Consequently, the absorption length is shorter and this allows the device to be thinner [4]. This, combined with a larger electron mobility, translates into shorter response times. However, to obtain low noise

*This article may be downloaded for personal use only. Any other use requires prior permission of the author and AIP Publishing. This article appeared in AIP Conference Proceedings 2054, 060064 (2019) and may be found at https://doi.org/10.1063/1.5084695.

APDs it is essential that the material feature very different electron and hole ionization coefficients [1]. While the ratio between these two coefficients in Si is greater than 20, in III-V compound semiconductors it is close to one. To solve the problem super-lattice structures consisting of nanometric-size alternating layers of compound semiconductors with different band gaps have been suggested in literature. This approach exploits the so-called "band gap engineering" techniques, which lead to the synthesis of multilayers with different composition and thus the modulation of the semiconductor band gap energy at the sub-nm level. Such approach would allow to minimize the multiplication noise [5].

DETECTOR GROWTH AND FABRICATION

The devices under investigation were grown epitaxially onto GaAs wafers by using molecular beam epitaxy (MBE) techniques. The photolitographic fabrication procedure applied to obtain the separated absorption and multiplication (SAM) APD is the one reported in [6]. A sketch of such device is shown schematically in Fig. 1. The absorption region is a 4.3-µm-thick layer of GaAs, while the multiplication region is composed of a staircase structure with 12 repetitions: each stage consists of 35 nm of GaAs, 25 nm of $Al_{0.45}Ga_{0.55}As$ and 20 nm of a linearly graded region formed by a digital alloy (a sequence of GaAs/$Al_{0.45}Ga_{0.55}As$ bilayers with thickness ratios giving variable average composition from 0.45 to 0). These two regions are separated by a δ p-doped layer of carbon atoms characterized by a concentration of $2.5 \cdot 10^{12}$ cm^{-2}. At the end of the fabrication process, the structures feature a mesa of 600 µm and an opening of 350 µm in diameter.

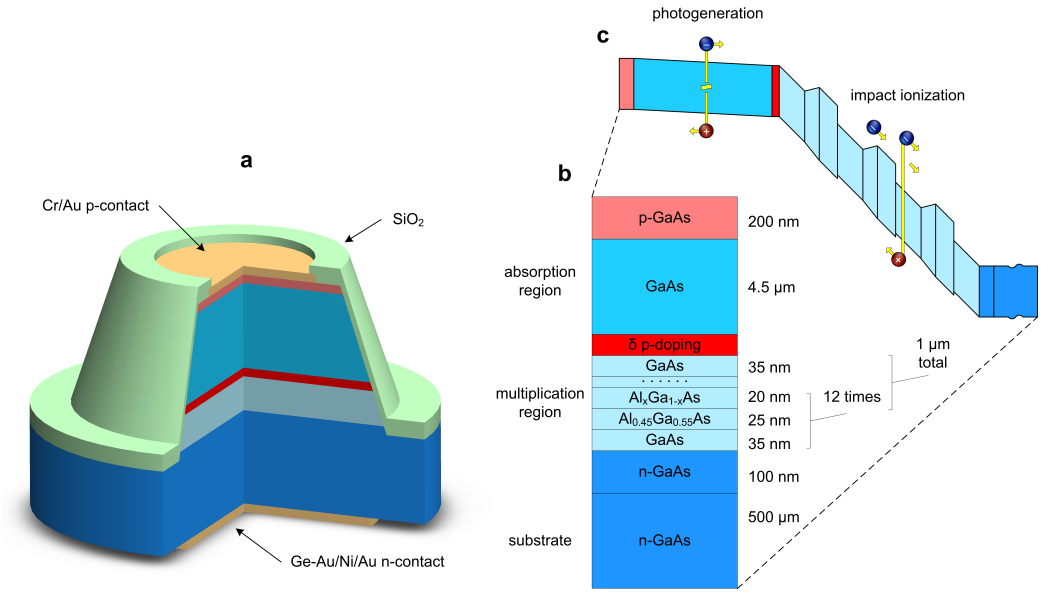


FIGURE 1. (a) Sketch of the fabricated avalanche photodiode with separated absorption and multiplication regions. (b) Scheme of the structure grown by MBE. (c) Band diagram under reverse bias.

EXPERIMENTAL RESULTS

Electrical Characterization

In a first step, the devices have been characterized by measuring capacitance-voltage (CV) and current-voltage (IV) curves. For practical reasons we report here just the representative results of one of the devices.

The CV measurements were performed through a precision LCR meter (HP4284A) at 1 MHz. Figure 2a shows the results of these measurements (black circle) compared to a TCAD [7] simulation of the structure under test (red

curve with triangles). From the experimental curve it is possible to calculate the width of the depletion region as

$$d = \frac{\varepsilon_r \varepsilon_0 A}{C},$$

where A is the area of the mesa, C is the measured capacitance, $\varepsilon_r = 12.6$ [8] and $\varepsilon_0 = 8.854 \cdot 10^{-12}$ F/m are the equivalent relative permittivity of the active region (calculated as the average value of the permittivity of the different materials in the depletion region) and the permittivity of vacuum, respectively. From this calculation a depth of the depletion region of 1 μm is obtained. This value corresponds to the depth of the multiplication region, showing as expected that only this portion of the device is depleted.

Dark current-voltage measurements, instead, have been carried out inside a black box in air and at room temperature. The reverse IV curve is displayed as black circles in Fig. 2b and reveal a breakdown voltage of 38 V.

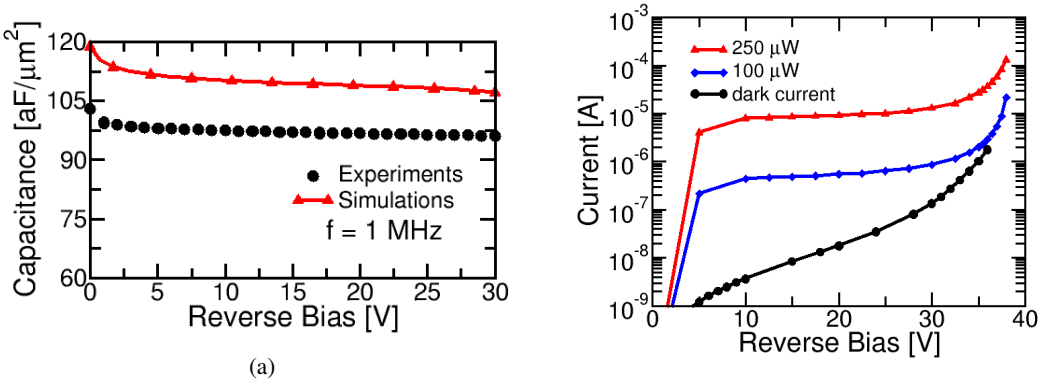


FIGURE 2. (a) Comparison between experimental (circles) and simulated CV characteristic of the staircase SAM APD (triangles) with a δ layer concentration of $2.5 \cdot 10^{12}$ cm^{-2}. (b) Measurements performed in a black box at atmospheric pressure and at room temperature with a laser source: black circles, dark current; blue diamonds, laser power of 100 μW; red triangles, 250 μW.

Noise Measurements with Laser

Set-up

The system built for measuring gain (M) and excess noise factor (F) was based on a transimpedance amplifier (TIA), which converts the current of the photo-detector into a more convenient voltage signal. In particular, the set-up to measure both F and M was realized by feeding simultaneously the output of the TIA into a spectrum analyser (Agilent EXA Signal Analyzer N9010A) and an oscilloscope (LeCroy HDO6104), whose input resistance was set to 1 MΩ. The spectrum analyzer was fore-run by a 470-nF capacitor to avoid any issue with the DC compliance of the instrument input. The TIA features a transimpedance of 10 kΩ and a frequency cut above 1.5 MHz, achieved for an input capacitance of 50 pF (cable, set-up and 30-pF device). A block diagram of the measurement system is shown in Fig. 3.

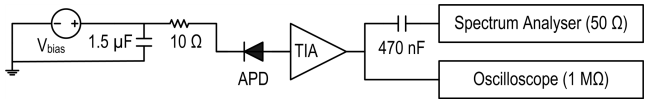


FIGURE 3. Block diagram of the system.

For these measurements the device was kept in a stainless steel and UHV compatible chamber, which in turn was placed into a dark box, whereas the APD was illuminated by a tabletop laser ($\lambda = 532$ nm). The green laser was

selected such that the photo-induced charge generation was limited to the absorption region only [6], so as to have ideal conditions of charge injection close to the entrance window in the absorption region during noise characterisation. For all measurements reported here, the laser spot was always focused on the centre of the device opening. To reduce pick up from the power supply (HP E3631A, ±25 V cascaded) the device was biased through a CR filter (1.5 μF, 10 Ω). The resistor was chosen such that the bias drop across it could be neglected even for the largest expected photocurrent.

The TIA was used to convert the APD current into a proportional voltage, which possesses information about the noise generated by the device under test (DUT). In fact, the noise generated under illumination is expected to differ from the noise under dark conditions and therefore this difference can be used to elucidate the noise associated with the avalanche gain process which multiplies the photocurrent [9].

Results

Several IV curves under laser light illumination have been acquired utilizing a four channel picoammeter (AH501) and are reported in Fig. 2b tuning the laser power to 100 μW (blue diamonds) and 250 μW (red triangles). In addition dark current measurements are shown as well (black circles).

The currents and the noises measured while the device was illuminated by the laser were used to calculate M and F. Figure 4a shows the gain as a function of the bias. Different curves are displayed: the symbols (triangles and diamonds) represent the measured gain of the DUT for different laser powers. The gain is defined as

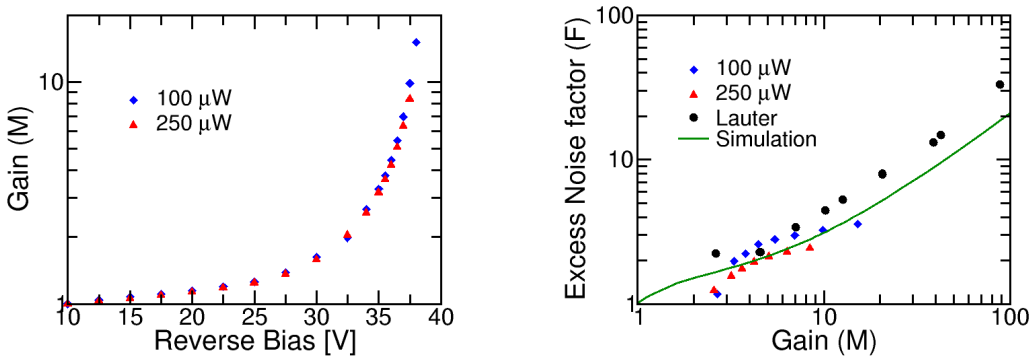
$$M = I_{ph}/I_{pho} \tag{1}$$

where I_{ph} is the difference between the measured photocurrent and the current measured under dark conditions and I_{pho} is the photocurrent at unity gain. It can be seen that the gains calculated for different powers are almost coincident over the evaluated range of voltages.

The excess noise factor F can be defined through the ratio between the power spectral density of the photogenerated current ($S_{ii,ph}$) and the power spectral density of the shot noise ($S_{ii,shot}$):

$$\frac{S_{ii,ph}}{S_{ii,shot}} = \frac{2qIRFM^2}{2qIR} = FM^2 \tag{2}$$

where q is the elementary charge, I is the photocurrent at unity gain and R is the load resistance.



(a) (b)

FIGURE 4. (a) Measured gain versus voltage for the staircase SAM APD: blue diamonds, 100 μW; red triangles, 250 μW. (b) Excess noise factor as a function of the gain: the green line is the simulated curve, while the symbols are the measured values.

In order to validate the excess noise estimations obtained through the laser measurements, the resulting values of F were compared with the ones obtained by simulating the nominal structure with the Energy Balance History-Dependent (EBHDM) model (presented in [10], with the nominal device parameters as in [11]), as well as with other experimental results reported in literature for a structure very similar to the one fabricated in this work [11]. Figure 4b compares these results by plotting F as a function of M. It can be observed that the values (blue diamonds, 100 μW

and red triangles, 250 μW) obtained with the set-up described in Fig. 3 follow the trend suggested by the EBHDM simulations (green curve) fairly good even at different laser powers; furthermore, over the entire evaluated range of gains the excess noise of the DUT does not exceed the levels reported in the aforementioned literature.

X-ray Measurements

Set-up

To assess the response to high photon energy, the devices were tested under irradiation with hard X-rays generated by the XRD2 wiggler beamline at Elettra Sincrotrone Trieste [12] (12.4 keV and $1.7{\cdot}10^{13}$ph·s^{-1} over an area of 300x90 μm^2).

For tests under illumination the devices were mounted on a dedicated, 4-channel printed circuit board (PCB) and accommodated in the aforementioned UHV-compatible chamber, which was placed downstream in the focal plane of the XRD2 line. The photocurrents generated in the devices were measured utilizing the aforementioned AH501. Owing to incorporated perpendicular movement stages it was possible to perform remotely controlled spatial mesh scans of the devices through the beam with a spot of approximately 100x100 μm^2 and a typical photon flux in the order of 10^{12}ph·s^{-1}. Various mesh scans were performed in order to evaluate the homogeneity of the generated photocurrent over the entire surface of the device. The scans were acquired with a step of 30 μm.

Furthermore, such photocurrent maps were used to align the center of the DUT with the incident radiation to record position invariant IV measurements and to perform time measurements. These were carried out by using an oscilloscope (KEYSIGHT DSOS404A) with 4 GHz bandwidth, a sample rate of 20 GSa·s^{-1} and a 10-bit resolution.

Results

Figure 5 reports the IV curves for both dark current and responses to different photon fluxes, which were adjusted at different values by means of Al absorbers. In order to avoid radiation damage to the device the power provided by the synchrotron beamline was kept at least an order of magnitude below the ones emitted by the laser source, Fig. 2b. In any case for both sources we observe the same expected behaviour showing an increase in current with the increase of incident power.

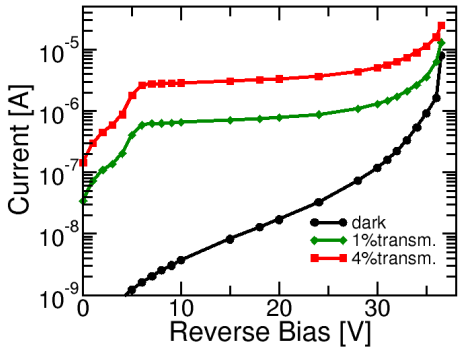
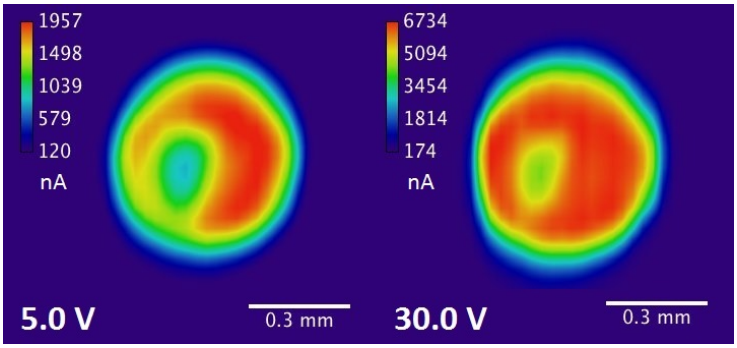


FIGURE 5. Measurements performed in air with a hard X-ray beam provided by the XRD2 beamline: black circles, dark current; green diamonds, 1% of transmitted beam through an Al filter; red squares, transmission 4%.

Moreover, the IV curve under illumination follows quantitatively the expected progression of a SAM APD: recombination ($V_{bias} < 4$V), unity gain (4V $< V_{bias} <$ 7V), punch through ($V_{bias} \approx 7$V), where all charges generated in the absorption region are transferred into the multiplication region, then the avalanche region (7V $< V_{bias} <$ 38V) and eventually breakdown ($V_{bias} > 38$V) after which the device can operate in Geiger mode.

This is also shown in the different photocurrent maps acquired with 12.4-keV photons at the XRD2 beamline using two different bias voltages (Fig. 6a, 6b). At 5.0 V, in the recombination regime, the charge collection efficiency is low. In the avalanche region at higher reverse biases (e.g. 30.0 V) the photocurrent maps becomes fairly uniform (systematic error of 10^{-2} in comparison to the stochastic error of 10^{-5}) indicating maximum charge collection beyond the punch through voltage. The area of lower efficiency (bottom left) is the absorption of the wire bond.



(a) (b)

FIGURE 6. XY scans performed in air, with a hard X-ray source (12.4 keV) and with different bias voltages (a,b).

Preliminary time measurements were carried out, showing that these devices achieve a rising time of approximately 150 ps. Moreover, during these measurements at 12.4 keV the radiation hardness was tested. In fact, the DUTs were exposed to a 6 mW flux for approximately 10 hours and further measurements showed that they do not exhibit any perceivable damage or variation in the performances.

CONCLUSIONS

Several SAM APDs were grown using MBE techniques, electrically characterised and tested at room temperature and in air under two different light sources, respectively, with a green laser (2.33 eV) and with synchrotron radiation (12.4 keV). The estimated excess noise factor as function of the gain approached the simulated results, and the devices at higher energy had the expected behaviour for different powers. In future, new devices characterized by smaller areas, thus lower capacitances and more controlled dark currents, will be fabricated. Moreover, thicker absorption region based on Cr-compensated GaAs wafer [13] will allow to create e-h pairs only in the absorption region, creating thus the optimal condition to have less noise also when using higher energies.

ACKNOWLEDGEMENTS

The research in this work received funding by the Italian MIUR through the PRIN 2015 project 2015WMZ5C8. Furthermore, the authors would like to thank the personal of the XRD2 beamline for the opportunity to perform measurements at high energy and G. Bais, A. Heroux and D.G. Dumitrescu for their support during the experiments.

REFERENCES

[1] R. McIntyre, *IEEE Electr. Device Lett.*, **46**, 1623 – 1631 (1999).
[2] P. Yuan, K. Anselm, C. Hu, H. Nie, C. Lenox, A. Holmes, B. Streetman, J. Campbell, and R. McIntyre, *IEEE Trans. Electron. Devices*, **46**, 1632 – 1639 (1999).
[3] J. Hubbell, *Int. J. Appl. Radiat. Isot.*, **33**, 1269–1290 (1982).
[4] J. Lauter, D. Protic, A. Forster, and H. Luth, *Nucl. Instr. and Meth. A*, **356**, 324–329 (1995).
[5] F. Capasso, *IEEE Trans. Nucl. Sci.*, **30**, 424 – 428 (1983).
[6] T. Steinhartova, C. Nichetti, M. Antonelli, G. Cautero, R. Menk, A. Pilotto, F. Driussi, P. Palestri, L. Selmi, K. Koshmak, S. Nannarone, F. Arfelli, S. Dal Zilio, and G. Biasiol, *J. Instrum.*, **12**, p. C11017 (2017).
[7] Synopsys, sentaurus^{TM} device user guide, 2006.
[8] M. Levinshtein and S. Rumyantsev, *Handbook Series on Semiconductor Parameters*, Vol. 1 (1996), pp. 1–32.
[9] K. S. Lau, C. Tan, B. Ng, K. Li, R. Tozer, J. David, and G. Rees, *Meas. Sci. Technol.*, **17**, p. 1941 (2006).
[10] C. Nichetti, A. Pilotto, P. Palestri, L. Selmi, M. Antonelli, F. Arfelli, G. Biasiol, G. Cautero, F. Driussi, Y. Klein, R. H. Menk, and T. Steinhartova, *IEEE T. Electron Dev.*, **65**, 1823–1829 (2018).
[11] J. Lauter, A. Forster, H. Luth, K. Muller, and R. Reinartz, *IEEE Trans. Nucl. Sci.*, **43**, 1446 – 1451 (1996).

[12] XRD2, "Elettra and FERMI lightsources," (2018).
[13] M. Veale, S. Bell, D. D. Duarte, M. French, M. Hart, A. Schneider, P. Seller, M. Wilson, V. Kachkanov, A. Lozinskaya, V. A. Novikov, O. P. Tolbanov, A. Tyazhev, and A. N. Zarubin, *J. Instrum.*, **9**, p. C12047 (2014).